Journal of Cleaner Production 252 (2020) 119829

Contents lists available at ScienceDirect

Journal of Cleaner Production

journal homepage: www.elsevier.com/locate/jclepro

Sizing a renewable microgrid for flow shop manufacturing using climate analytics

Vinod Subramanyam, Tongdan Jin*, Clara Novoa

Ingram School of Engineering, Texas State University, San Marcos, TX, 78666, USA

ARTICLE INFO

Article history:
Received 22 April 2019
Received in revised form
21 November 2019
Accepted 20 December 2019
Available online 23 December 2019

Handling editor: Prof. Jiri Jaromir Klemeš

Keywords:
Levelized cost of energy
Microgrid sizing
Renewable portfolio
Time-of-use
Flow shop scheduling
Climate analytics

ABSTRACT

A variety of methods have been proposed to assist the integration of microgrid in flow shop systems with the goal of attaining eco-friendly operations. There is still a lack of integrated planning models in which renewable portfolio, microgrid capacity and production plan are jointly optimized under power demand and generation uncertainty. This paper aims to develop a two-stage, mixed-integer programming model to minimize the levelized cost of energy of a flow shop powered by onsite renewables. The first stage minimizes the annual energy use subject to a job throughput requirement. The second stage aims at sizing wind turbine, solar panels and battery units to meet the hourly electricity needs during a year. Climate analytics are employed to characterize the stochastic wind and solar capacity factor on an hourly basis. The model is tested in four locations with a wide range of climate conditions. Three managerial insights are derived from the numerical experiments. First, time-of-use tariff significantly stimulates the wind penetration in locations with medium or low wind speed. Second, regardless of the climate conditions, large-scale battery storage units are preferred under time-of-use rate but it is not the case under a net metering policy. Third, wind- and solar-based microgrid is scalable and capable of meeting short-term demand variation and long-term load growth with a stable energy cost rate.

1. Introduction

It is estimated that manufacturing industry world-wide is responsible for over one-third of electricity consumption (EIA, 2017). This is mainly due to the adoption of energy-intensive production equipment, and the use of heating, ventilation and air conditioning systems. A typical semiconductor wafer fab that runs in 24/7 mode requires 400 to 700 MWh of electricity per day, which results in $15–25 million of annual utility cost (Hu and Chuah, 2003; ITRS, 2011). To generate this amount of electricity, every day over 300 metric tons of carbon have to be released if burning fossil fuels. To achieve the environmental sustainability, various approaches have been proposed, ranging from energy conservation (Liu et al., 2013, 2014; Mouzon et al., 2007), power efficiency (Aflaki et al., 2013; Chen et al., 2013; Li and Sun, 2013), renewable energy purchase (Jin et al., 2018), and onsite generation (Ghadimi et al., 2013; Ruangpattana et al., 2011). The common feature of these approaches is to reduce the conventional electricity use in manufacturing processes. In addition, manufacturing plants opt to participate in demand response programs and shift their loads from peak hours to off-peak hours for cost savings (Bego et al., 2014; Wang and Li, 2013; Zhang et al., 2017b). Time-of-use tariff, critical peak pricing, and real-time pricing are among the common demand response programs used in industrial facilities.

Biel and Clock (2016) point that most production planning models focus either on long-term or on short-term scheduling problems, but the decisions on renewable portfolio, microgrid capacity, and manufacturing schedule are rarely studied in a unified framework. Such a joint planning realistically represents the opportunity a manufacturer can take when facing multiple energy supply options. In fact, most papers make use of energy-related objectives aiming to minimize the energy consumption or cost with the implicit assumption that the energy source or the generation capacity is known. However, due to the intermittency of renewables and the lack of large-scale, cost-effective energy storage technology, manufacturers have to consider the unique characteristics of the local wind and weather profiles in order to harvest onsite energy at a minimum cost. Thus, neither the renewable portfolio nor its associated capacity can be treated as known parameters. Rather the planners should identify the best generation

* Corresponding author.
E-mail address: tj17@txstate.edu (T. Jin).

https://doi.org/10.1016/j.jclepro.2019.119829
0959-6526/

mix that leads to higher renewable throughput based on the specific wind and weather condition of that area.

This paper attempts to address two research questions: First, how to model and design an integrated microgrid and flow shop production system given multiple renewable resources with uncertain climate conditions? Second, is it economically viable to install wind, solar and storage systems to attain eco-friendly operation considering demand response and load growth? To address both questions, an integrated planning model is proposed to jointly size a renewable microgrid and to schedule the flow shop production by minimizing the levelized cost of energy (LCOE) over one year horizon. LCOE is the cost of generating one MWh or kWh electricity, and is widely used to measure the market competitiveness of different generation technologies with different lifetime.

The contribution of this study can be elaborated in three aspects. First, the paper makes an early attempt to concurrently allocate microgrid capacity and production schedule subject to power demand and supply uncertainty. Particularly the model includes investment decisions on a portfolio of wind, solar and energy storage to match the uncertain demand with variable supply during the course of a year. Second, the model takes into account cost savings and revenue from selling surplus energy to the utility grid under demand responses. It combines the operational (short-term) decision with the strategic (long-term) planning by matching, on an hourly basis, the uncertain load with the variable generation. Third, the paper employs a climate analytics approach to characterizing the hourly capacity factor of wind turbine (WT) and photovoltaics (PV) systems based on 11-year meteorological data. This data analytics approach factors the operational and strategic decisions in the LCOE metric through the aggregation and minimization of annualized energy costs. This allows the manufacturers to realistically evaluate the economic viability of adopting and integrating onsite renewables in flow shop manufacturing.

The remainder of the paper is organized as follows. Section 2 provides the literature review. In Section 3, a two-stage, mixed-integer optimization model is formulated to minimize the LCOE. Section 4 presents the climate analytics approach based on 11-year, hourly meteorological data. In Section 5, the proposed model is tested in four locations with a wide range of climate profile. Section 6 performs the sensitive analysis with respect to capacity cost, operating mode and microgrid scalability. Section 7 concludes the paper.

2. Literature review

Flow shop scheduling is a special case of job shop planning where there is a strict order for all jobs to be performed on a set of machines in an appropriate sequence. Flow shop scheduling problems with single and multiple objectives under different design criteria have been extensively studied. The majority of flow shop scheduling problems are formulated to minimize the makespan (Benavides and Ritt, 2018; Marichelvam et al., 2014), flowtime (Dong et al., 2013), tardiness (Liu et al., 2014), and release date (Bai et al., 2017). Interested readers are referred to the survey papers by May el al. (2015), Ruiz and Vázquez-Rodríguez (2010), and Yenisey and Yagmahan (2014).

Recently a growing number of flow shop scheduling models focus on minimizing energy costs through load shifting, production adjustment, and buffer building under various demand response programs. Wan and Qi (2010) attempt to schedule a single machine under a variable electricity price with the goal of minimizing total energy cost. More general and complex manufacturing systems, such as multi-stage and multi-machine shops, have been investigated for lowering energy cost subject to time-varying electricity rate. For instance, Shrouf et al. (2014) extend the single-machine model and use the genetic algorithm to find the near optimal solution that is applicable to large-scale manufacturing scheduling problems. Zhang et al. (2014) propose a scheduling optimization model to minimize the electricity cost and the carbon emissions in a three-stage flow shop under time-of-use (TOU) tariff. An unlimited buffer size between stages is assumed in their model. Wang and Li (2013) consider limited buffer sizes and solve a TOU-based flow shop scheduling problem to minimize the electricity cost subject to a fixed throughput requirement. Research efforts are also directed to other electricity pricing schemes such as critical peak pricing. Bego et al. (2014) investigate the scheduling problem for a multi-stage production system where machines and buffers are under critical peak pricing. More recently, Liu et al. (2018) deign a flexible flow shop for recycling reinforced composite materials by minimizing both time and energy, and the optimal schedule is found by using non-dominated sorting genetic algorithm. These studies have shown that demand response is an effective way to reduce the energy cost if the schedules or capacities of a production system can be adjusted in a real-time manner.

The second research stream focuses on integrating distributed or onsite renewable power in flow shop production scheduling systems. The purpose is to reduce the energy cost or grid electricity use subject to variable power and time-dependent utility price. For example, Moon and Park (2014) make an early attempt to minimize the total production cost of a flexible job shop scheduling problem by combining time-dependent electricity price, energy storage and distributed wind- and solar power. Zhang et al. (2017a) minimize the electricity cost of a flow shop powered by grid-tied microgrid comprised of photovoltaics and energy storage. Biel et al. (2018) propose a decision support model for flow shop scheduling problem with a grid-tied wind turbine using a stochastic mixed integer linear programming. They show that onsite wind generation can significantly mitigate the influence of time-varying utility prices in the peak period. More recently Golpîra et al. (2018) introduce the smart energy-efficient production-planning concept for a job shop manufacturing system that is co-powered by the main grid and the microgrid. The latter is comprised of WT, storage device, and combined heat and power. A risk-based robust mixed integer linear program is formulated to minimize the day-ahead energy cost considering peak demand charge. The aforementioned studies show that a microgrid creates multiple benefits, including meeting demand responses, lowering carbon emissions, and improving energy security. The assumption of these studies is that the renewable portfolio or the microgrid capacity is known.

The third research stream also aims to integrate distributed wind and solar power into manufacturing facilities with minimum cost, but the main focus is on the sizing and siting of renewable resources by considering climate diversity and variability. At the plant level, Taboada et al. (2012) take an early step to optimize the capacity of a grid-tied, PV-based microgrid with the goal of meeting the hourly load of a wafer fab during the course of a year. The objective is to minimize the annualized energy cost of the microgrid, and the model is tested in five US cities with a wide range of weather profile. Villarreal et al. (2013) further expand the renewable portfolio and use WT as an alternative source to compensate the solar generation shortage in night time. Simulation-based optimization is used to find the optimal sizing of WT and PV that minimizes the system cost. At the machine level, Zhang et al. (2018) investigate a microgrid sizing problem for a diesel generator in a flow shop manufacturing setting subject to critical peak pricing rate. A mixed-integer non-linear programming model is formulated to optimize the generator capacity and the machine on-off policy by minimizing the sum of the utility and onsite generation cost. These studies indicate that it is of importance to determine the generation

portfolio and power capacity so as to maximize the throughput of onsite renewable or fuel-based generators in the presence of power demand and supply uncertainty.

The literature review shows that the majority of studies have focused on the coordination of production and power scheduling to lower the energy cost or to ensure the job throughput rate under various electricity tariffs. Efforts are also made to integrate wind and solar power in production models for reducing grid energy use with given renewable portfolio or capacity. However, there is a lack of an integrated framework in which renewable portfolio, generation capacity and flow shop scheduling are jointly considered under load and generation uncertainty. This paper proposes an integrated planning model to simultaneously size renewable capacity and allocate production schedule for minimizing the levelized cost of energy. The benefit of the joint planning model is to avoid or mitigate the under- or over-generation capacity investment by considering the unique wind and weather profiles of a particular location.

3. Joint allocation of microgrid and production schedule

3.1. Flow shop system with microgrid generation

As shown in Fig. 1, the microgrid under study consists of WT, solar PV, battery storage (BS) units, and the flow shop facility acting as the load. This paper investigates a grid-tied microgrid system by considering two operational scenarios. In scenario one, if the wind blows hard or the sunshine is strong, the microgrid is able to energize the flow shop with no reliance on the main grid. If surplus power is generated, it can be stored in the BS unit or fed in the main grid if the battery is full. In scenario two, if the aggregate wind and solar power is less than the load, the BS behaves as complementary energy source to co-power the flow shop. Situations may also occur when the main grid power must be purchased if the BS energy is depleted.

A machine flow shop system refers to the process in which all jobs, also known as work-in-process (WIP), have a unidirectional and fixed processing route. Without loss of generality, the three-stage, parallel machine shop system in Fig. 1 is used to illustrate the working principle. After the initial jobs enter Stage 1, they are processed on machine 1 or 2. Upon completion, they are stored temporally in buffer 1. Once machine 3 or 4 is available, these WIP will be fed to Stage 2 for further processing. Buffer 2 is used to store the finished WIP from Stage 2. Finally the jobs are processed on machine 5 or 6 at Stage 3, and the finished goods are stored in buffer 3. This paper seeks an optimal schedule for a multi-product, multi-period flow shop system to minimize the annual energy consumption while satisfying the required throughput rate.

3.2. Flow shop scheduling for energy minimization

Let us consider a hybrid flow shop with n jobs being processed at stage $s \in S$ for $S = \{1, 2, \ldots, d\}$ where d is the total number of stages. A buffer with a capacity of C_s is placed at the end of stage s. Each stage consists M_s parallel machines. Also, the set of time periods $\mathcal{T}_f = \{t_0,\ t_0+1, .., t_0+T_p\}$ has specific time instances, where t_0 is the initial time at which a machine begins to operate and T_p is the planning horizon or the total available production time. The essential throughput for job $j \in J$ is notated as h_{j0} for the given time period $\mathcal{T}_f$. The flow of jobs is done in feed-forward control from the first to the last stage. Table 1 summarizes the notation for the multi-stage, parallel machine scheduling model.

Each machine is either in on- or off-mode depending on the maintenance status. The time and electric power required for processing job j on machine m in stage s are T_{smj} and P_{smj}, respectively. Since the machines within a stage are identical, their processing speeds are the same for the same job type. Nevertheless the model formulated below can also be extended to machines with different processing speeds. This paper also considers the machine maintenance action, and v_{sm} is the maintenance time for machine m in stage s. Based on the previous works (Zhang et al. 2017a; Zhang and Chiong, 2016), a flow shop scheduling model, denoted as Model 1, is presented to minimize the annual energy use under the throughput requirement.

Model 1 (Stage 1 Decision):

Minimize:

$$f_1(\mathrm{x}) = \sum_{t=1}^{T_p} \sum_{s=1}^{d} \sum_{m=1}^{M_s} \sum_{j=1}^{n} P_{smj} x_{smjt} \tag{1}$$

Subject to:

$$N_{sjt} = 0 \quad \text{for} \quad j \in J; s \in S; t = t_0, \ldots, t_0 + w_{smj} - 1; \tag{2}$$

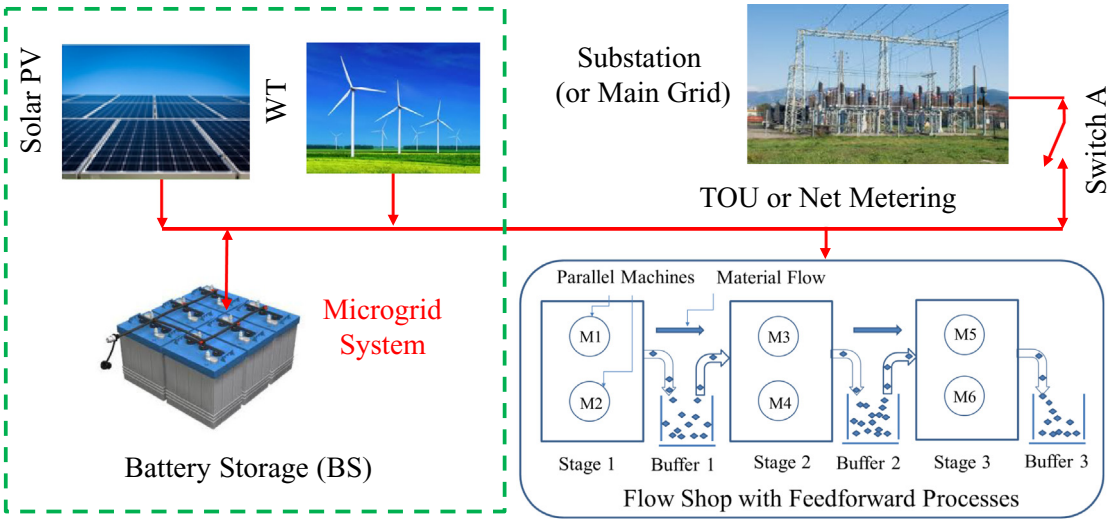

Fig. 1. A flow shop system integrated with microgrid.

Table 1
Notation for machine flow shop scheduling problem.

Indexes and Parameters	
k	: index to represent the cumulative production hours, for $k = 1, 2, \ldots, T_p$ t:: index to represent time
d	: number of stages
s	: stage index, for $s = 1, 2, \ldots, d$
m	: machine index
n	: number of jobs
j	: job type index for $j = 1, 2, \ldots, n$
M_s	: number of parallel machines in stage s, for $m = 1, 2, \ldots, M_s$
$\mathscr{T}_f$	: set of time instances in machine operational interval, $\mathscr{T}_f = \{ t_0, t_0 + 1, \ldots, t_0 + T_p \}$ where t_0 is the start time and T_p is the end operating time
h_{j0}	: required throughput rate for job j
w_{smj}	: time required for processing job j on mahcine m in stage s
P_{smj}	: power consumed for processing job j on machine m in stage s
v_{sm}	: time required for maintenance of machine m in stage s
C_s	: buffers capacity in stage s
Decision Variables:	
x_{smjt}	: 1, if machine m at stage s is processing job j at time t, and 0 otherwise
y_{smjt}	: 1, if machine m in stage s starts processing job j at time t, and 0 otherwise
N_{sjt}	: amount of products of type j being processed in stage s by time t
$\bar{x}_{smt}$	: 1, if machine m in stage s at time t is under maintenance , and 0 otherwise
$\bar{y}_{smt}$	: 1, if machine m in stage s at time t starts the maintenance , and 0 otherwise

$$N_{sjt} = \sum_{k=0}^{t-w_{smj}+1} y_{smjk} \quad \text{for} \quad j\in J; s\in S; t = t_0 + w_{smj}, \ldots, t_0 + T_p; \tag{3}$$

$$N_{sjt} \geq N_{s+1,jt} + x_{s+1,mjt} \quad \text{for} \quad j\in J; s\in S\backslash\{d\}; t\in \mathscr{T}_f; \tag{4}$$

$$N_{sjt} \leq N_{s+1,jt} + C_s \quad \text{for} \quad j\in J; s\in S\backslash\{d\}; t\in \mathscr{T}_f; \tag{5}$$

$$N_{djT_p} \geq h_{j0} \quad \text{for} \quad j\in J; \tag{6}$$

$$x_{smjt} = \sum_{k=0}^{t} y_{smjk} \text{ for } j\in J; s\in S; m\in M_s; t = t_0 \ldots, t_0 + w_{smj} - 1; \tag{7}$$

$$x_{smjt} = \sum_{k=t-w_{smj}+1}^{t} y_{smjk} \quad \text{for} \quad j\in J; s\in S; m\in M_s; t = t_0, \ldots, t_0 + T_p; \tag{8}$$

$$\sum_{k=t}^{t+w_{smj}-1} x_{smjk} \geq y_{smjt} w_{smj} \quad \text{for} \quad j\in J; s\in S; m\in M_s; t = t_0, \ldots, t_0 + T_p - w_{smj} + 1; \tag{9}$$

$$\sum_{j\in J} x_{smjt} \leq 1 \quad \text{for} \quad s\in S; m\in M_s; t\in \mathscr{T}_f; \tag{10}$$

$$\sum_{j\in J} y_{smjt} \leq 1 \quad \text{for} \quad s\in S; m\in M_s; t\in \mathscr{T}_f; \tag{11}$$

$$\bar{x}_{smt} = \sum_{k=0}^{t} \bar{y}_{smk} \quad \text{for} \quad m\in M_s; t = t_0 \ldots, t_0 + v_{sm} - 1; \tag{12}$$

$$\bar{x}_{smt} = \sum_{k=t-v_{sm}+1}^{t} \bar{y}_{smk} \text{ for } s\in S; m\in M_s; t = t_0 + v_{sm}, \ldots, t_0 + T_p; \tag{13}$$

$$\sum_{k=t}^{t+v_{sm}-1} \bar{x}_{smk} \geq \bar{y}_{smt} v_{sm} \text{ for } s\in S; m\in M_s; t = t_0, \ldots, t_0 + T_p - v_m + 1; \tag{14}$$

$$\bar{x}_{smt} + \sum_{j\in J} x_{smjt} \leq 1 \quad \text{for } s\in S; m\in M_s; \ t\in \mathscr{T}_f; \tag{15}$$

$$x_{smjt},\ y_{smjt} \in \{0,1\} \quad \text{for } j\in J; s\in S; m\in M_s; t\in \mathscr{T}_f; \tag{16}$$

$$\bar{x}_{smt},\ \bar{y}_{smt} \in \{0,1\} \quad \text{for } s\in S; m\in M_s; t\in \mathscr{T}_f; \tag{17}$$

$$N_{sjt} \in \mathbf{Z} \quad \text{for} \quad j\in J; s\in S; t\in \mathscr{T}_f; \tag{18}$$

Table 2
Notation for microgrid capacity allocation model.

Parameters		**Comments**
P_D^t	:	Power demand of the flow shop at time t
R_g^t	:	the TOU rate at time t
$Pmax_{CS}$	:	the maximum power that the battery can be charged
$Pmax_{DS}$	:	the maximum power that the battery can discharge
η_{CS}	:	charging efficiency of battery system
η_{DS}	:	discharging efficiency of battery system
ϕ_{PV}	:	capital recovery factor of PV system
ϕ_{WT}	:	capital recovery factor of WT system
ϕ_B	:	capital recovery factor of battery system
a_{PV}	:	capicity cost for PV system
a_{WT}	:	capicity cost for WT system
a_B	:	capicity cost for battery system
P_i^t	:	power charged to the battery at time t
P_o^t	:	power discharged from the battery at time t
P_g^t	:	power drawn from the main grid at time t
P_{PV}^t	:	power output of the PV at time t
P_{WT}^t	:	power output of the WT at time t
P_S^t	:	enegry stored in the battery at the end of the interval of t
CS_t	:	charging status at time t. $CS_t = 1$ if the battery is charging, and 0 otherwise
DS_t	:	discharging status at time t. $DS_t = 1$ if the battery is discharging , and 0 otherwise
λ_{PV}^t	:	capacty factor of PV at time t
λ_{WT}^t	:	capacty factor of WT at time t
Decision Variables:		
P_{PV}^c	:	capacity of the PV system
P_{WT}^c	:	capacity of the WT system
P_B^c	:	capacity of the batterysystem

The objective function (1) aims to minimize the total energy use of the flow shop during the entire production period. Particularly, the objective function aggregates the energy demand of n jobs being processed across all the machines in each stage over period $\mathscr{T}_f$. Constraints (2) and (3) ensure the number of jobs being processed by time t does not exceed the machine capacity in each stage. Constraints (4) represents the job balance equation, that is, the number of processed jobs in stage s should not be less than the sum of the processed jobs in stage s+1 and those are under processing at stage s+1. Constraints (5) indicates that at any time t, the number of processed jobs at stages s should be less than the sum of processed jobs in stage s+1 and the buffer capacity at stage s, or the overflow occurs. Constraint (6) is the throughput requirement, stating that the total finished job j should not be less than the target value h_{j0} by the end of period $t_0 + T_p$. Constraints (7) and (8) together ensure that job j under processing on machine m cannot be interrupted in duration w_{smj}. Constraint (9) stipulates that job j under processing on machine m must be completed in the same machine. Constraints (10) prescribes that at any time t, machine m can process at most one job. Constraints (11) prescribes that at any time t, machine m can start to process at most one job. Constraints (12) to (14) ensure the continuity of maintenance action with no interruption until completed. Constraint (15) stipulates that job processing and maintenance cannot be concurrently performed on the same machine. Constraint (16) simply states that at time t, there is at most one job being processed on machine m in stage s. Constraint (17) defines the fact that at time t, at most one maintenance task is applied to machine m in stage s. Finally, constraint (18) states that the job throughput should be a non-negative integer.

3.3. Optimal sizing of renewable microgrid

The next task is to determine the renewable portfolio and microgrid capacity to meet the power demand of the flow shop during the production period. The decision variables and model parameters for the second stage optimization are listed in Table 2 below.

Without loss of generality, the production planning horizon is taken as one year with $T_p = 8640$ h. Denoted as Model 2, the following optimization model is formulated to minimize the LCOE of the microgrid.

Model 2 (Stage 2 Decision):

Minimize:

$$f_2(P_{PV}^c, P_{WT}^c, P_B^c) = \frac{1}{f_1(\mathrm{x})}\left(\sum_{t=1}^{T_p} R_g^t P_g^t + \phi_{PV} a_{PV} P_{PV}^c + \phi_{WT} a_{WT} P_{WT}^c + \phi_B a_B P_B^c\right) \tag{19}$$

Subject to:

$$P_g^t + P_{PV}^t + P_{WT}^t - \frac{P_i^t}{\eta_{CS}} + P_o^t \eta_{DS} = P_D^t \quad for \quad t \in \mathscr{T}_f; \tag{20}$$

$$P_D^t = \sum_{s=1}^{d} \sum_{m=1}^{M_s} \sum_{j=1}^{n} P_{smj} x_{smjt} \quad for \quad t \in \mathscr{T}_f \tag{21}$$

$$P_{PV}^{t} = \lambda_{PV}^{t} P_{PV}^{c} \quad for \quad t \in \mathcal{T}_f ; \tag{22}$$

$$P_{WT}^{t} = \lambda_{WT}^{t} P_{WT}^{c} \quad for \quad t \in \mathcal{T}_f ; \tag{23}$$

$$0 \le P_S^t \le P_B^c \quad for \quad t \in \mathcal{T}_f ; \tag{24}$$

$$P_i^t \le Pmax_{CS} \times CS_t \quad for \quad t \in \mathcal{T}_f ; \tag{25}$$

$$P_o^t \le Pmax_{DS} \times DS_t \quad for \quad t \in \mathcal{T}_f ; \tag{26}$$

$$P_S^{t-1} - P_S^t = P_o^t - P_i^t \quad for \quad t \in \mathcal{T}_f ; \tag{27}$$

$$CS_t + DS_t \le 1 \quad for \quad t \in \mathcal{T}_f ; \tag{28}$$

$$CS_t , \ DS_t \in \{0, 1\} \quad for \quad t \in \mathcal{T}_f ; \tag{29}$$

$$P_g^t \ge 0; \tag{30}$$

$$P_{PV}^c , \ P_{WT}^c , \ P_B^c \ge 0. \tag{31}$$

The objective function (19) aims to minimize the LCOE where $f_1(\mathbf{x})$ is the total energy use of the flow shop in period T_p, which is the result of Model 1. The numerator represents the annual electricity cost of the flow shop. Particularly the first summation is the utility bill, and the last three summations in (19) represent the annualized equipment cost including operations and maintenance expense. Note that ϕ_{PV}, ϕ_{WT} and ϕ_B are the capital recovery factor of PV, WT, and BS, respectively. Constraints (20) shows that at any time t, the aggregate power of the main grid, PV, WT, and BS equals the demand of the flow shop. The power demand is given in Constraint (21) where x_{smjt} is resulted from Model 1. Constraints (22) and (23) define the output power of PV and WT at time t based on the hourly capacity factor. Constraint (24) states that the amount of energy stored in BS at time t should not exceed its capacity limit. Constraints (25) and (26) define the maximum amount of power charged or discharged at time t from the battery. Constraint (27) is the BS energy balance equation showing that the net energy between time t-1 and t equals the difference between the discharged and charged energy in that period. Constraint (28) ensures that battery charge and discharge cannot take place simultaneously. Constraints (29) and (30) simply stipulate the non-negativity of all the decision variables.

Table 3
Average wind speed at 80m height and weather condition (2006–2016).

Cities	Wellington	Aswan	Yuma	San Francisco
Latitude (Degree)	41.29	24.09	32.69	37.77
Average Wind Speed (m/s)	13.61	5.93	6.02	8.21
Clear Sky	6	356	165	28
Scattered Cloud (SC)	68	5	109	95
Partially Cloudy (PC)	109	3	65	136
Mostly Cloudy (MC)	5	0	0	13
Overcast	1	0	0	2
Rain	170	0	13	65
Fog	2	0	1	24
Strom/T-storms	3	0	11	3
Snow	0	0	0	0
Wind Speed Profile	High	Low	Low	Medium
Sunshine	Low	High	High	Medium

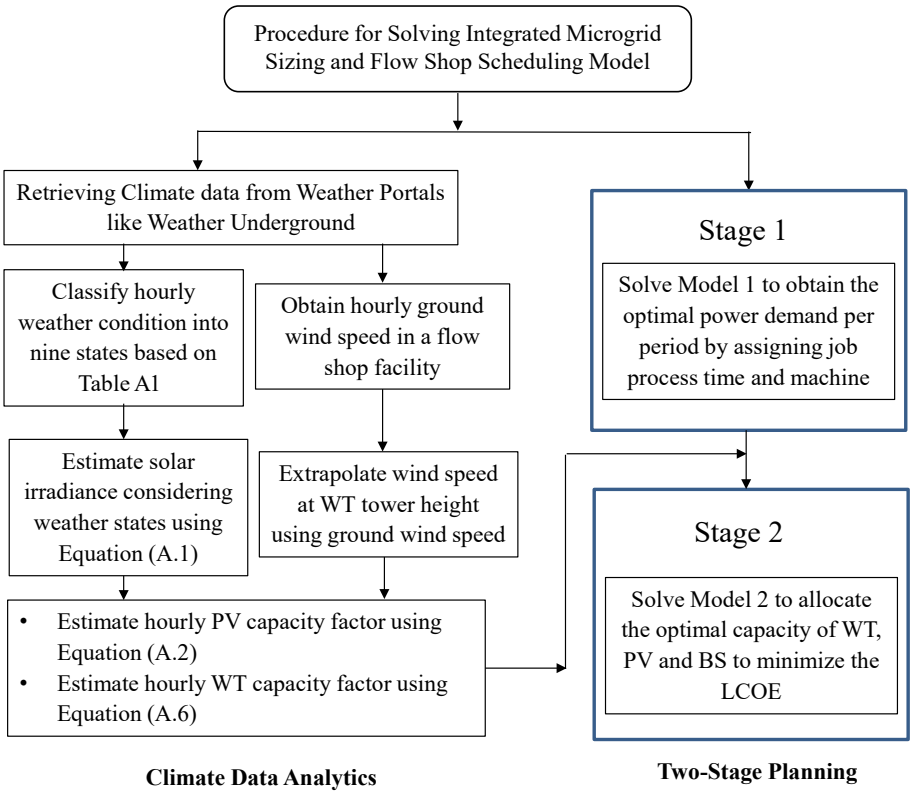

Fig. 2. Flow chart for solving the two-stage optimization.

3.4. Solution algorithm

Models 1 and 2 are mutually correlated in terms of the power demand and utility pricing policy. The power demand derived from Model 1 for each period becomes an input parameter of Model 2 decision. Both models are coded with the AMPL mathematical programming language and solved with the CPLEX search engine that has mixed integer linear programming solution algorithms. Similar to the production-logistics planning model by Pham et al. (2019), Fig. 2 describes the procedure for solving the two-stage, flow shop scheduling and microgrid sizing problem.

4. Climate analytics for capacity factor estimation

4.1. Climate data of testing cities

Four cities with diverse wind and weather conditions are chosen to test the proposed models in Section 3. They are Wellington in New Zealand, Aswan in Egypt, Yuma in Arizona, and San Francisco in California. For each city, wind speed data between 2006 and 2016 are retrieved from the Weather Underground portal (WU, 2018), and used to estimate the WT capacity factor. In particular, 96,360 hourly wind speed readings are collected for each city, and a total of 385,440 data points are used for the hourly capacity factor estimation. Similarly, the hourly weather states from 2006 to 2016 are also obtained from the portal with 96,260 readings per city and a total of 384,440 records are used for PV capacity factor estimation. By aggregating all the wind and weather records, the size of the dataset for the climate analytics reaches 770,880.

Table 3 summarizes the climate statistics of four cities between 2006 and 2016. Since the wind speed data from the weather portal are measured at 10m above the ground, they are extrapolated at 80m as this is the typical tower height of modern WT system. The weather conditions are classified into nine states, namely, clear sky, scattered cloud, partially cloudy, mostly cloudy, overcast, rain, fog, storm (including T-storm) and snow. Wellington has a strong wind profile with average wind speed (AWS) of 13.61 m/s at the height of 80m tower, but only 6 clear days per annum on average. Aswan has an extremely strong sunshine with 356 clear days, but the AWS is only 5.93 m/s. Yuma has a low wind profile of 6.02 m/s on average, but the number of the clear and scatter cloudy days reaches 274 days. San Francisco has a medium wind profile of 8.21 m/s, and the number of clear and scattered cloudy days reaches 123 per annum. The climates of these cities are relatively diverse, representing the areas where the human beings choose to live.

4.2. Capacity factor of WT and PV

Constraints (22) and (23) of Model 2 contain random capacity factors $\lambda_{PV}^{t}$and λ_{WT}^{t} resulted from stochastic climate conditions. To make the optimization tractable, both constraints are converted into deterministic forms by substituting the random capacity factors with their expected values derived from the climate analytics. The detailed procedure to estimate λ_{PV}^{t} and λ_{WT}^{t} is given in Appendix A. Figs. 3 and 4 depict the expected value of $\lambda_{PV}^{t}$and λ_{WT}^{t}, respectively, in Wellington, Aswan, Yuma and San Francisco. Since there is no PV generation in the night, Fig. 3 only shows the PV capacity factors in the day time of a year.

5. Numerical experiments

5.1. Background of the flow shop system

A three-stage hybrid flow shop system with parallel machines is adopted to demonstrate the application of Models 1 and 2. The experiment is built upon the flow shop system for semiconductor manufacturing. Table 4 presents a sample case for power demand and processing time of individual jobs which are related to wafer fabrication. The power demand in wafer processing is typically at the MW level (Hu and Chuah, 2003). For the job processing time, a fab takes 1–2 days or sometimes longer to process a complex layer on a particular machine or tool (ITRS, 2011; Mitra et al., 2012). Buffers with a reasonable size are placed between two adjacent stages. The flow shop produces two types of products (or jobs), and runs in three shifts in 24 h and seven days a week. The job processing time and the power used by each machine are listed in Table 4. For instance, {1, 2, 2} means if job 1 is processed on machine 2 at the second stage, the power demand is 3 MW and it takes 60 h to complete Job 1. The time-period is $\mathcal{T}_f = \{0, 1, \ldots, 8640\}$ assuming 30 days/month for twelve months. When maintenance is taken, the duration is assumed to be 2 h per machine, but it could be a different duration. According to the analysis by Hu and Chuah

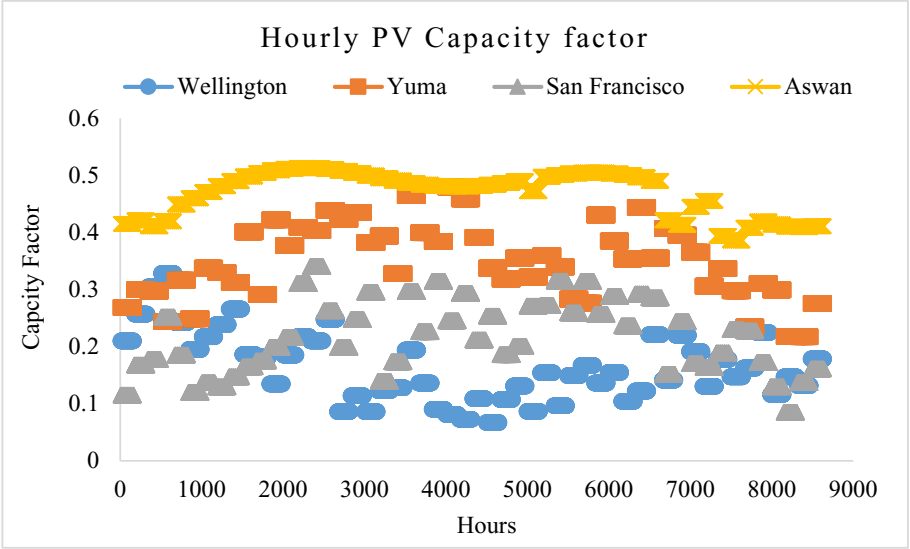

Fig. 3. PV capacity factor for four cities.

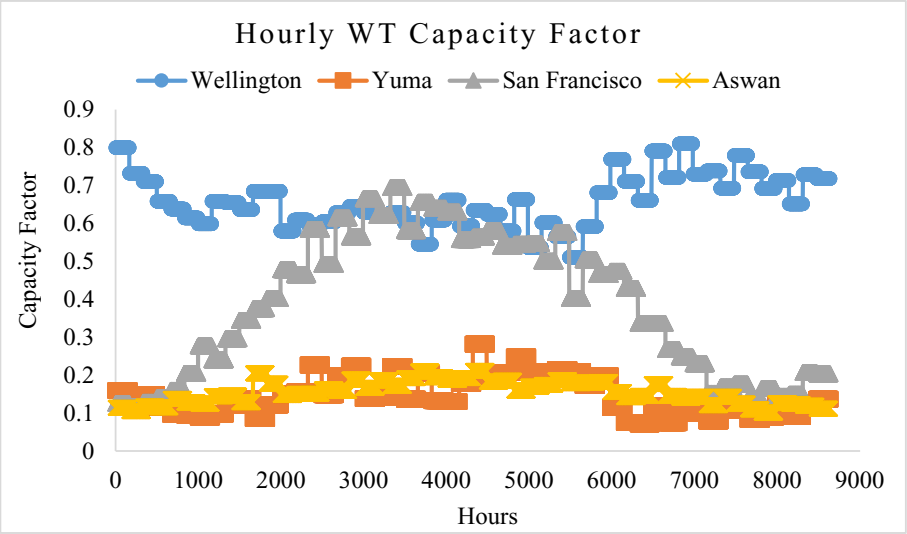

Fig. 4. WT capacity factor for four cities.

Table 4
Job processing power and time at different stages.

{Job, Stage, Machines}	Power Use (MW)	Processing Time (hour/Job)
{1, 1, 1}	3	40
{1, 1, 2}	4	40
{1, 1, 3}	4	40
{1, 2, 1}	3	60
{1, 2, 2}	3	60
{1, 2, 3}	4	60
{1, 3, 1}	3	40
{1, 3, 2}	4	40
{1, 3, 3}	4	40
{2, 1, 1}	4	40
{2, 1, 2}	3	40
{2, 1, 3}	4	40
{2, 2, 1}	4	60
{2, 2, 2}	5	60
{2, 2, 3}	4	60
{2, 3, 1}	3	40
{2, 3, 2}	4	40
{2, 3, 3}	4	40

(2003), the baseload typically is 3–5% of the mean load of a facility. Without loss of generality, the baseload of the flow shop is assumed to be 1 MW for keeping the lights on, and running air ventilation and other basic functions in the facility.

The flow shop model is solved in two production scenarios as shown in Table 5. Scenario 1 serves as the benchmark in which the monthly throughput of both jobs is at the regular level. Model 1 allocates the production schedule of Jobs 1 and 2 to meet the required throughput with minimum energy consumed over twelve months. In scenario 2, the throughput of each job doubles, and Model 1 is solved again to obtain the optimal production schedule at the high throughput level. In Scenario 1, there are two parallel machines in each stage, and in Scenario 2, three parallel machines

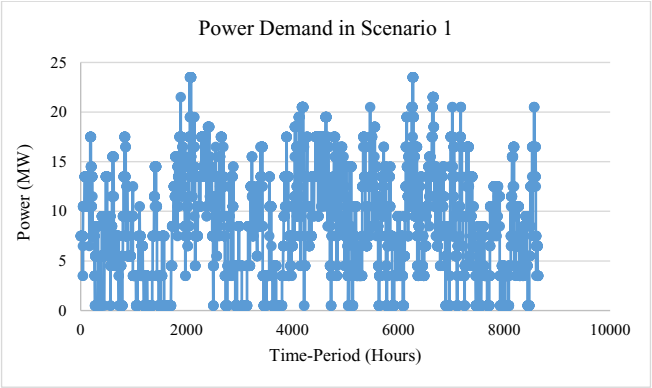

Fig. 5. Results of model 1 in scenario 1 production.

are used in each stage because of the high throughput requirement. In both scenarios, the buffer size of stages 1 and 2 is five, and the buffer size in the last stage is unlimited.

5.2. Results of flow shop scheduling

Model 1 is coded in AMPL mathematical programming language using the CPLEX solver running in an Intel(R) Core (TM) i7-8550U processor, which runs at 1.8 GHz and 24 GB DRAM. The current optimization model has approximately 674,000 integer decision variables and over 952,000 constraints during $T_p = 8640$ h. It takes about 38 min for the CPLEX solver to find the optimal solution for Model 1.

Scenario 1 is solved on an hourly basis, and the results of power demand are plotted in Fig. 5. By summing the hourly demand, the annual energy use reaches 75,928.5 MWh. It is also observed that

Table 5
Required throughput for each month.

Production Scenario	Jobs/WIP	Month											
		1	2	3	4	5	6	7	8	9	10	11	12
1	Job 1, Job 2	4	4	5	5	5	6	6	7	7	6	5	4
2	Job 1, Job 2	8	8	10	10	10	12	12	14	14	12	10	8

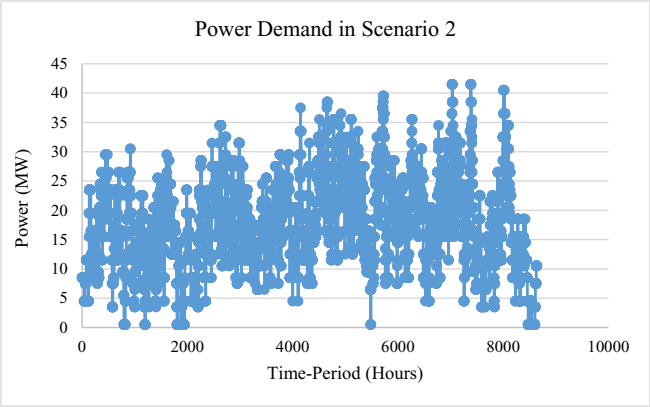

Fig. 6. Results of model 1 in scenario 2 production.

Table 6
Baseline parameters of WT, PV and BS for model 2.

Notation	Value	Comment
α_{PV}	$3.0M/MW	PV capacity cost
α_{WT}	$1.5M/MW	WT capacity cost
a_{BS}	$0.5M/MWh	BS capacity cost
ϕ_{PV}	0.0802	PV with 20-year lifetime, and 5% discount rate
ϕ_{WT}	0.0802	WT with 20-year lifetime, and 5% discount rate
ϕ_{BS}	0.1295	BS with 10-year life, and 5% discount rate
R_g	$70/MWh	Net-metering with flat rate
R_g	$70/MWh	Off-peak price from 10pm to 6am in TOU tariff
R_g	$140/MWh	Peak price from 7am to 9pm in TOU tariff
η_{CS}	0.9	Battery charging efficiency
η_{DS}	0.9	Battery discharging efficiency

the flow shop system experiences two peak demands that occur in hours 2074 and 6,268, requiring as much as 23.5 MW.

Similarly, Model 1 is solved in Scenario 2 under high throughput rate. The resulting power demand is presented in Fig. 6. It shows that the annual energy use reaches 153,720.5 MWh, which is twice of the use in Scenario 1. This result is expected because of the doubled throughput rate. However, in Scenario 2, the peak demand occurs in hours 7032 and 7382 with 41.5 MW, which differs from the occurrence time in Scenario 1. In Scenario 2, the minimum power demand of the facility is the same as in Scenario 1, but the frequency of machines in off state is smaller than in Scenario 1. This is also expected because in Scenario 2 machines are expected to stay on line longer to meet the high throughput rate.

5.3. Input data for microgrid sizing

Table 6 lists the values of the input parameters for Model 2. The baseline capacity cost for PV and WT is $3M/MW and 1.5M/MW, respectively. The capital recovery factor for PV and WT is computed by assuming 20 years lifetime with 5% annual discount rate (Fu et al. 2018a; Stehly et al., 2018). The baseline BS capacity cost is 0.5M/MWh. The BS capital recovery factor is estimated based on ten years lifetime with 5% discount rate, and the efficiency of battery charge η_{CS} and discharge η_{DS} is taken as 90% (Fu et al. 2018b). The nominal grid price is $70/MWh in net-metering. The TOU rate is $70/MWh in the off-peak period and $140/MWh in the peak period (Anderson et al., 2017). Fees associated with maintenance and land lease for equipment placement are factored into the capacity cost.

Model 2 is solved in four different cities: Wellington, Aswan, Yuma and San Francisco. For each city, both net-metering and TOU

Table 7
Eight different cases for model 2 in scenario 1 production.

City	Case No.	Pricing Policy	Production Scenario	Battery Cost
Wellington	1	Net-Metering	1	varies from $0.01M/MWh to $0.5M/MWh for all eight cases
Wellington	2	TOU	1	
Aswan	3	Net-Metering	1	
Aswan	4	TOU	1	
Yuma	5	Net-Metering	1	
Yuma	6	TOU	1	
San Francisco	7	Net-Metering	1	
San Francisco	8	TOU	1	

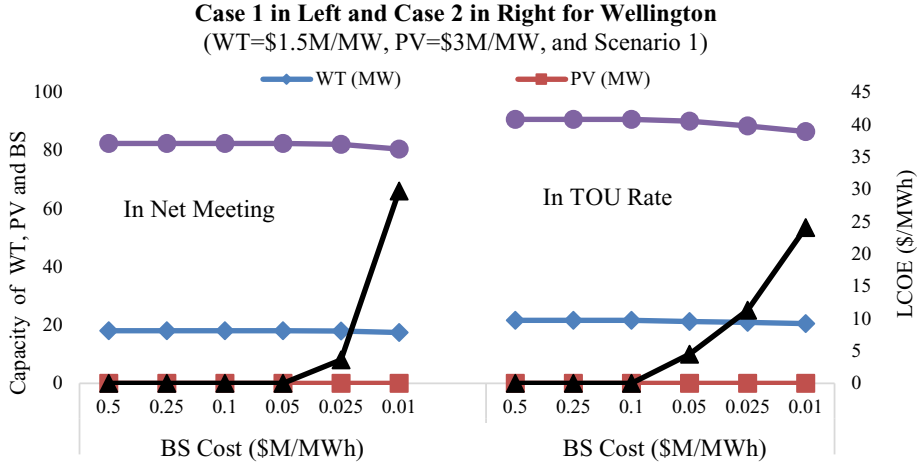

Fig. 7. Results of model 2 for scenario 1 production in wellington.

Fig. 8. Results of model 2 for scenario 1 production in aswan.

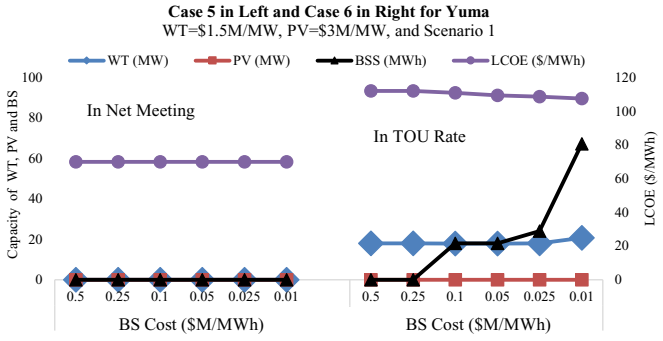

Fig. 9. Results of model 2 for scenario 1 production in yuma.

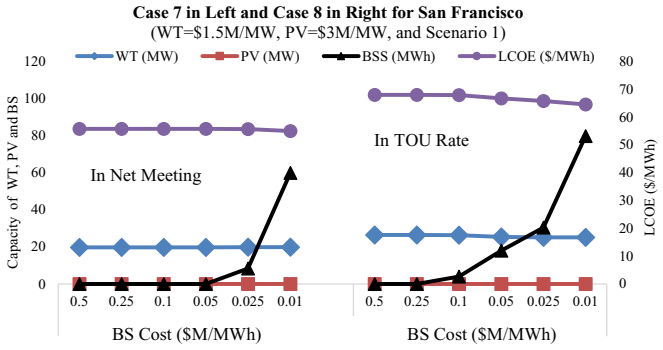

Fig. 10. Results of model 2 for scenario 1 production in san francisco.

rates are considered, which results in a total of eight cases in Table 7. In all eight cases, the flow shop operates subject to Scenario 1 throughput, hence the power demand curve in Fig. 5 is taken as the input for Model 2. For each case, Model 2 is solved repeatedly by reducing the BS cost from $0.5M/MWh to $0.01M/MWh, while the capacity costs for PV and WT remain the same. The optimal sizing of PV, WT and BS are found to minimize the LCOE.

5.4. Optimal microgrid sizing

AMPL mathematical programming language and the CPLEX solver are used to solve Model 2 which runs in an Intel(R) Core (TM) i7-8550U processor. The model contains three continuous decision variables and over 77,762 constraints. It takes about 13.4 min for the CPLEX solver to find an optimal solution for an instance of Model 2.

First, Model 2 is solved for Wellington based on the parameters in Tables 6 and 7 The optimal sizing for WT, PV, BS systems and LCOE under net metering and TOU rates are depicted in Fig. 7. The microgrid opts to install 18.05 MW wind capacity under net-metering, and 21.6 MW wind capacity in TOU rate. There is no PV installation in both pricing policies. The BS is chosen only when its cost drops below $0.05M/MWh in net-metering, and $0.1M/MWh in TOU. It is also found that the capacity of WT and BS in net-metering is smaller than that in TOU. LCOE in net metering is also smaller than that in TOU rate, and they are far below $70/MWh in both cases, indicating that wind power is very competitive in Wellington with 13.61 m/s at the 80-m turbine height.

Next Model 2 is solved for Aswan corresponding to Cases 3 and 4. Fig. 8 presents the optimal sizing of WT, PV and BS and the LCOE in net metering and TOU, respectively. In net metering neither WT nor PV is chosen, rather all the electric power is supplied from the main grid. As a result, there is no necessity to install the BS as well. In TOU, wind generation is preferred over PV, and wind capacity of 23.9 MW−26 MW turns out to be optimal depending on the BS cost. BS is chosen only if the cost drops below $0.25M/MWh in TOU. LCOE in net metering equals $70/MWh because of no installation of WT and PV. The LCOE in TOU varies between $105/MWh and $110/MWh, smaller than the peak rate of $140/MWh.

Now Model 2 is solved for Yuma corresponding to Cases 5 and 6, and the results are depicted in Fig. 9. With the capacity cost of $1.5M/MW for WT and $3M/MW for PV, it is more economical to use grid power in net-metering. Hence there is no installation of WT, PV and BS units. In TOU, however, wind generation becomes competitive, and the optimal WT size varies from 18 MW to 21 MW depending on the BS cost. Meanwhile, BS becomes competitive when its cost drops below $0.25M/MWh. LCOE in net metering is

equal to the grid price of $70/MWh because no WT, PV and BS are installed. LCOE in TOU tariff varies between $107/MWh and $112/MWh, yet smaller than the peak price of $140/MWh.

Finally, Model 2 is solved for San Francisco corresponding to Cases 7 and 8, and the results are shown in Fig. 10. In net metering, the wind generation is preferred with an installed capacity of 19.8 MW. The BS is chosen if its cost drops below $0.05M/MWh. Under TOU rate the installed wind capacity varies between 25.2 MW and 26.5 MW depending on the BS cost. The BS is chosen only if its cost drops below $0.25M/MWh. There is no PV installation in both cases. LCOE in net metering is also smaller than that in TOU. In net metering the LCOE is $55.0–55.8/MWh, and in TOU it is within $64.5–68.0/MWh, all below the nominal rate of $70/MWh, indicating that wind generation is very competitive in San Francisco given average wind speed of 8.21 m/s.

6. Sensitivity analysis

6.1. The impact of PV cost

Sensitivity analysis is performed by reducing the PV cost from $3M/MW to $1.5M/MW while keeping other parameters unchanged. Model 2 is solved again in four cities under net metering and TOU rates, respectively. Table 8 summarizes the new results in comparison with the outcomes of Cases 1–8. In the table the unit for WT and PV is $M/MW, and for LCOE is $/MWh.

It is observed that in net metering, the renewable portfolio of the microgrid remains the same in Wellington, San Francisco, and Yuma even if the PV cost is down by 50%, but the solar generation becomes competitive in Aswan where 7–9 MW PV is installed along with 22.9 MWh BS capacity. Under TOU rate with the PV cost of $1.5M/MW, it is found that Aswan and Yuma becomes favorable to PV generation. In particular, Aswan chooses to install 19.8–21.4 MW PV by displacing the wind generation. Yuma also gives up wind generation, and opts to install 17.2–20.3 MW PV depending on the BS cost. Under TOU rate, wind power in Wellington and San Francisco remains competitive even if the PV cost is down to $1.5M/MW.

6.2. The impact of demand response program

This section analyzes the impact of electricity pricing policy on the sizing of WT, PV and BS units. Assume the net meeting rate is increased from $70/MWh to $140/MWh. Model 2 is solved for four cities with WT cost of $1.5M/MW and PV cost of $3M/MW. The results are summarized in Fig. 11 along with those from Cases 1, 3, 5, and 7. A common observation is that the capacity of WT, PV ad BS increases in all cities with the growth of utility price. For instance, given $0.01MW/MWh cost of BS system in San Francisco, the WT size goes up from 19.9 to 27.8 MW, and the BS goes up from 59.9 to 94.MWh. Both Aswan and Yuma do not choose wind and solar power if the utility price is $70/MWh. However, wind generation is preferred in both cities if the utility price reaches $140/MWh. The conclusion is that a higher utility price stimulates the adoption of onsite renewable generation, which is in alignment with the intuition.

Model 2 is also solved for four cities under the TOU rate in which the off-peak price increases to $140/MWh between 10pm and 6am, and the peak price is $210/MWh between 7am and 9pm. The results are shown in Fig. 12 in comparison to Cases 2, 4, 6, and 8. A common observation is that the WT and BS capacity increases with the escalated TOU rate across four cities. In fact the WT capacity is more than doubled in Aswan and Yuma. This experiment clearly indicates that a higher TOU rate in peak hours significantly stimulates the adoption and use of WT in areas with medium or low wind speed.

6.3. Microgrid scalability

To examine whether the microgrid system is scalable, Model 2 is solved under a higher power demand condition using Scenario 2 production data. The results for four cities are listed in Table 9 in comparision with those from Scenario 1. Two observations can be made. First, LCOE in Scenario 2 is equal to or less than the LCOE in Scenario 1 regardless the BS capacity cost. Second, the WT capacity in Scenario 2 is less than the twice of the WT size in Scenario 1, while the BS capacity in both scenarios remain almost the same. In

Table 8
Sensitivity analysis for PV cost in four locations.

City	BS Cost ($M/MWh)	PV Cost ($M/MW)	Net Meeting with Flat Rate				Time-of-Use Rate			
			WT	PV	BS	LCOE	WT	PV	BS	LCOE
Wellington	0.50	3	18.1	0	0	37	21.6	0.0	0	41
		1.5	18.1	0	0	37	21.6	0.0	0	41
	0.10	3	18.1	0	0	37	21.6	0.0	0	41
		1.5	18.1	0	0	37	21.6	0.0	0	41
	0.01	3	17.4	0	66.0	36	20.5	0.0	53.4	39
		1.5	17.4	0	66.0	36	20.5	0.0	53.4	39
Aswan	0.50	3	0	0	0	70	23.9	0	0	110
		1.5	0	7	0	69	0	19.8	0	99
	0.10	3	0	0	0	70	23.8	0	18	109
		1.5	0	7	0	69	0	21	18	96
	0.01	3	0	0	0	70	26	0	82	105
		1.5	0	9	22.9	69	0	21.4	51.4	92
Yuma	0.50	3	0	0	0	70	18	0	0	112
		1.5	0	0	0	70	2.2	17.2	0	108
	0.10	3	0	0	0	70	18	0	18	111
		1.5	0	0	0	70	0	19.3	18	106
	0.01	3	0	0	0	70	20.8	0	67.3	108
		1.5	0	0	0	70	0	20.3	51.9	102
San Francisco	0.50	3	19.8	0	0	56	26.5	0	0	68
		1.5	19.8	0	0	56	26.5	0	0	68
	0.10	3	19.8	0	0	56	26.3	0	4	68
		1.5	19.8	0	0	56	26.3	0	4	68
	0.01	3	19.9	0	59.9	55	25.2	0	79.8	65
		1.5	19.9	0	59.9	55	25.2	0	79.8	65

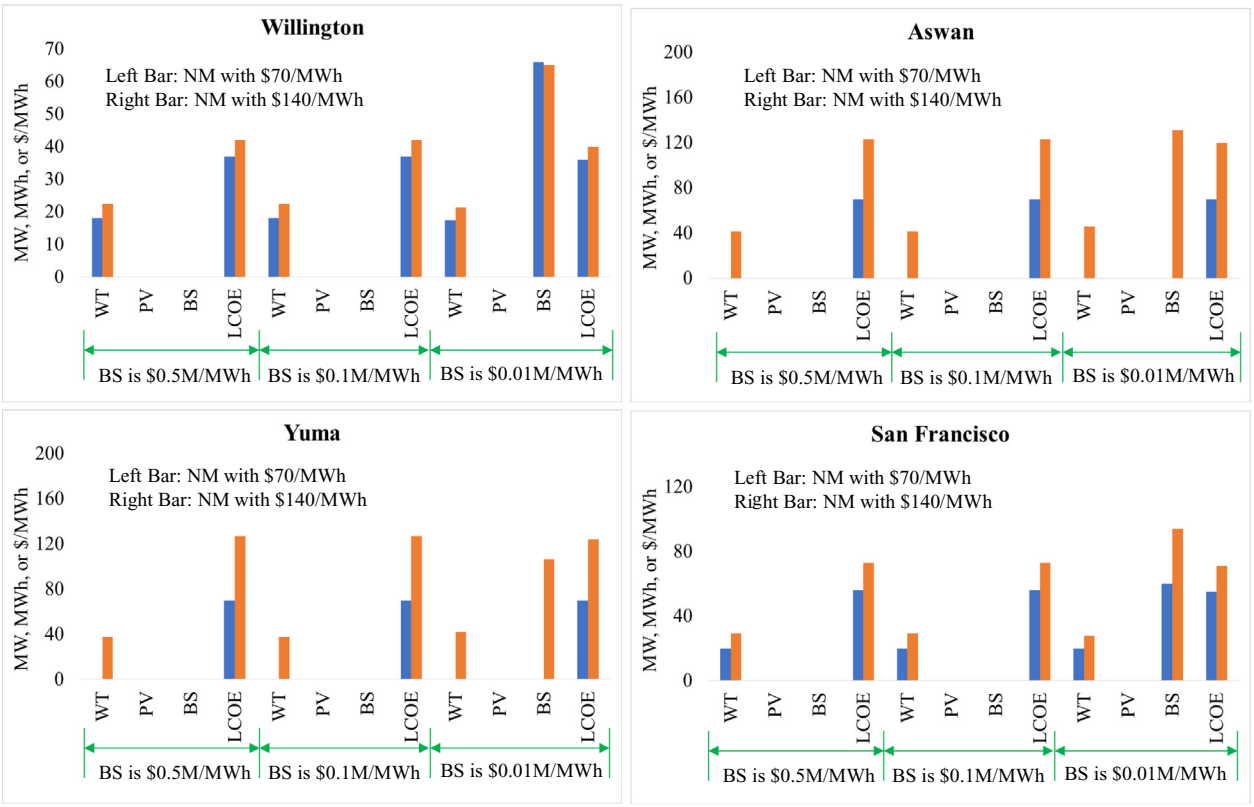

Fig. 11. The impact of net metering (NM) on Microgrid capacity.

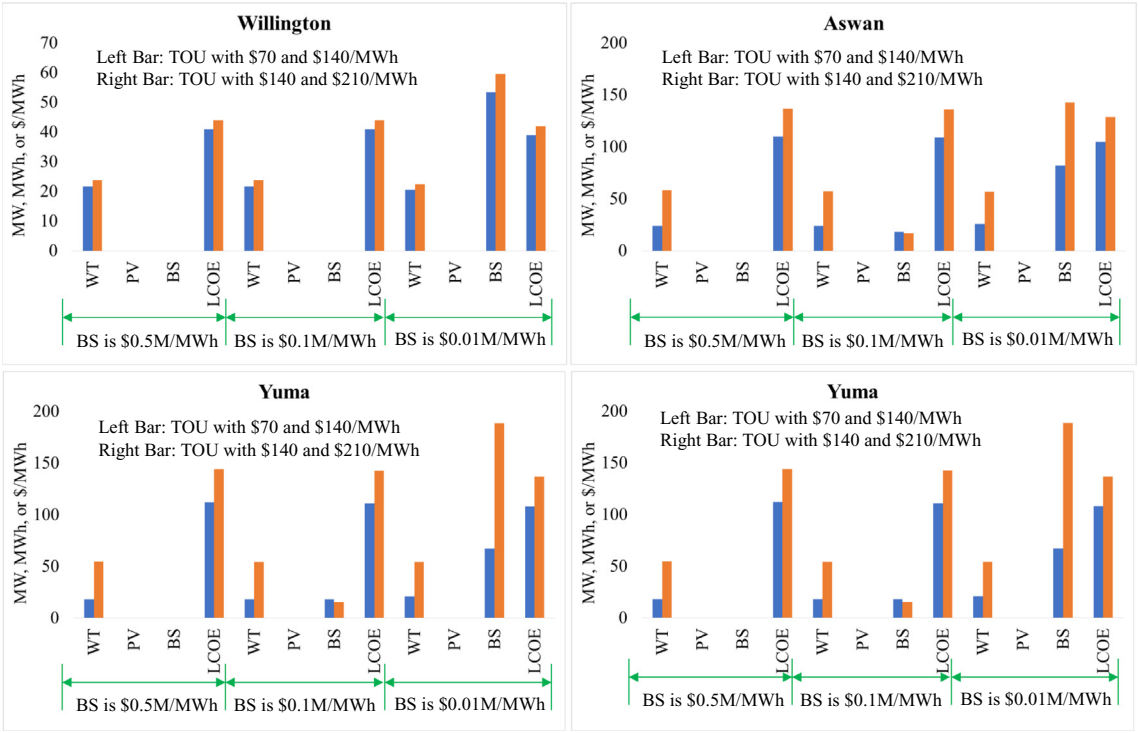

Fig. 12. The impact of TOU rate on microgrid capacity.

Wellington, for example, given the BS cost is $0.01M/MWh, the WT size in Scenario 1 is 17.4 MW and it is 32.7 MW in Scenario 2. The latter is less than the twice of the former. The BS capacity in Scenarios 1 and 2 is 66.1 MWh and 68 MWh, respectively, and both are very similar. Table 10 presents the optimal size of WT, PV and BS, and the LCOE value for Scenarios 1 and 2 under TOU tariff.

Table 9
Microgrid scalability under net metering program.

City	BS Cost	$0.5M/MWh				$0.1M/MWh				$0.01M/MWh			
	Scenario	WT	PV	BS	LCOE	WT	PV	BS	LCOE	WT	PV	BS	LCOE
Wellington	1	18.1	0	0	37	18.1	0	0	37	17.4	0	66.1	36
	2	32.7	0	0	32	32.7	0	0	32	32.5	0	68	32
Aswan	1	0	0	0	70	0	0	0	70	0	0	0	70
	2	0	0	0	70	0	0	0	70	0	0	0	70
Yuma	1	0	0	0	70	0	0	0	70	0	0	0	70
	2	0	0	0	70	0	0	0	70	0	0	0	70
San Francisco	1	19.8	0	0	56	19.8	0	0	56	19.9	0	59.9	55
	2	37.1	0	0	52	37.1	0	0	52	37.4	0	47.2	51

Table 10
Microgrid scalability under TOU tariff.

City	BS Cost	$0.5M/MWh				$0.1M/MWh				$0.01M/MWh			
	Scenario	WT	PV	BS	LCOE	WT	PV	BS	LCOE	WT	PV	BS	LCOE
Welling-ton	1	21.6	0	0	41	21.6	0	0	41	20.5	0	53.4	39
	2	37.7	0	0	35	37.4	0	1.67	35	36.1	0	59.7	34
Aswan	1	23.9	0	0	110	23.8	0	18	109	26.0	0	82.0	105
	2	70.8	0	0	104	71.9	0	18	103	74.8	0	76.5	101
Yuma	1	18.0	0	0	112	18.0	0	18	111	20.8	0	67.3	108
	2	60.3	0	0	108	62.2	0	18	107	64.1	0	57.5	106
San Francisco	1	26.5	0	0	68	26.3	0	4	68	25.2	0	79.8	65
	2	48.9	0	0	63	48.3	0	7.18	63	46.1	0	69.5	61

Similar observations can be made as those in Table 9. Hence the microgrid is scalable and able to accommodate long-term demand growth while maintaining a stable LCOE. Another observation is no significant increase of battery capacity under higher throughput rate.

6.4. The model limitations

The proposed model has several limitations that can be further improved. For instance, a constant machine maintenance time is assumed while in reality the downtime is uncertain depending on the maintenance policy (i.e. preventive or corrective). Besides, in the current model, wind, solar and battery units are the primary energy sources. The microgrid could be expanded to incorporate other energy forms such as small hydro, geothermal and combined heat and power. Finally, the scheduling model is based on a flow shop production with a fixed job sequence. More flexible production schemes, such as job shop scheduling and manufacturing cells are also desirable.

7. Conclusions

This study formulates and solves a two-stage, mixed-integer programming model for jointly allocating microgrid capacity and flow shop schedule over a year horizon. In stage 1, the job processing time and machines are assigned such that the total energy use over the year is minimized. In stage 2, a wind- and solar-based microgrid is sized to meet the hourly load subject to demand responses. The uniqueness is that the model seamlessly integrates the operational production plan with the strategic power capacity decision to achieve the environmental sustainability based on hourly climate analytics.The proposed model is tested in four locations with a wide range of climate conditions. To characterize the intermittent generation, a set of 0.77 million meteorological data across eleven years are used for estimating the hourly wind and solar capacity factors. Three managerial insights are derived from the numerical experiments. First, wind generation is cost-effective if the wind speed at the tower height exceeds 8 m/s, which has been demonstrated in Wellington and San Francisco. Second, the flow shop under time-of-use tariff is more desirable to adopt onsite wind and solar generation compared to the flat rate tariff. Third, giving the battery capacity cost of $0.5M/MWh, it is not economically attractive to the large-scale use of this technology. However, time-of-use tariff can stimulate the adoption of battery system if its cost drops to $0.25M/MWh. For future research, the flow shop scheduling model can be extended to a multi-facility production network that involves prosumer energy trading market. Incorporating other demand response programs such as real-time pricing is also an interesting direction.

Declaration of competing interest

None.

Acknowledgment

This project is supported by the National Science Foundation (NSF) under CBET Grant No. 1704933.

Appendix A. PV and WT Capacity Factor Estimation

A.1. PV Capacity Factor in Northern Hemisphere

The output power of PV system depends on multiple factors, including weather condition, operating temperature, and PV efficiency and size, among others. Let T_o, η, A, and I_t represent the operating temperature, PV efficiency, panel size, and solar irradiance incident on PV under the clear sky at time t. The actual output of a PV system considering the weather uncertainty can be estimated as

$$P_t = W_t \eta A I_t [1 - 0.005(T_o - 25)] , \quad (A.1)$$

where P_t is the actual output power of the PV system (unit: Watt) at time t, and W_t is the weather factor that varies between 0 and 1 to mimic different weather states (Lave and Kleissl, 2011). The values

of W_t associated with nine weather states are summarized in Table A1 where SC is for scattered cloud, PC is for partially cloudy, and MC is for mostly cloudy.

Table A1
Weather Factor in Different Weather States

No.	1	2	3	4	5	6	7	8	9
State	Clear Sky	SC	PC	MC	Overcast	Rain	Fog	Storm	Snow
W_t	1	0.7	0.5	0.3	0.2	0.1	0.1	0.1	0

The PV capacity factor at time t can be estimated by

$$\lambda_{PV}^{t} = \frac{1}{P_{PV}^{c} \times K} \sum_{k=1}^{K} P_t, \quad \text{for } t = 1, 2, \ldots, \mathrm{T_p} \tag{A.2}$$

Where P^{c}_{PV} is the maximum or rated capacity of a PV system, and K is the number of years under study. In this study the value of K is 11 years.

A.2. Wind Turbine Capacity Factor

A WT system possess four operating phases depending on the wind speed v against the turbine blades. Let $P_w(v)$ be the instantaneous output of a WT at v. Then the cubic power curve is given as (Thiringer and Linders, 1993).

$$P_w(v) = \begin{cases} 0 & v < v_c, \ \ v > v_s \\ P_{WT}^{c}(v/v_r)^3 & v_c \le v \le v_r \\ P_{WT}^{c} & v_r \le v \le v_s \end{cases} \tag{A.3}$$

where v_c, v_r and v_s stand for the cut-in, the rated, and the cut-off speed, respectively. Though variations may exist, for modern WT systems, $v_c = 3$ m/s, $v_r = 12$ m/s, and $v_s = 25$ m/s. Note P^{c}_{WT} is the rated WT capacity. Wind speed at a particular time can be fit with Weil distribution (Bilir et al., 2015). The probability density function and the distribution function are given below

$$f_w(v) = \frac{k}{c}\left(\frac{v}{c}\right)^{k-1} e^{-(v/c)^k}, \quad \text{for } v \ge 0 \tag{A.4}$$

$$F_w(v) = e^{-(v/c)^k}, \quad \text{for } v \ge 0 \tag{A.5}$$

where c and k are the scale and shape parameters, respectively. Then the WT capacity factor at time t can be estimated as (Novoa and Jin, 2011)

$$\lambda_{WT}^{t} = \frac{E[P_w(V)]}{P_{WT}^{c}} = \frac{1}{v_r^3} \int_{v_c}^{v_r} v^3 f_w(v) dv + (F_w(v_s) - F_w(v_r)) \,, \tag{A.6}$$

where V is the random wind speed and v is its realization. The values of λ_{PV}^{t} and λ_{WT}^{t} always fall in the range of [0, 1].

Author contribution sections

Vinod Subramanyam: The main contribution is the preliminary computation, algorithm implementation, and the preparation of 55% draft manuscript. Tongdan Jin: The contribution includes the model formulation, climate data analytics, and revising and expanding the manuscript. Clara Novoa: The contribution includes the model checking, computational assistance in AMPL, and revising the manuscript.

References

Aflaki, S., Kleindorfer, P.R., Sáenz de Miera Polvorinos, V., 2013. Finding and implementing energy efficiency projects in industrial facilities. Prod. Oper. Manag. 22 (3), 503–517.

Anderson, K., Cutler, D., DiOrio, N., Butt, B., Richards, A., 2017. Increasing resiliency through renewable energy microgrids. J. Energy. Manag. 2 (2), 22–39.

Bai, D., Liang, J., Liu, B., Tang, M., Zhang, Z.-H., 2017. Permutation flow shop scheduling problem to minimize nonlinear objective function with release dates. Comput. Ind. Eng. 112 (October issue), 336–347.

Bego, A., Li, L., Sun, Z., 2014. Identification of reservation capacity in critical peak pricing electricity demand response program for sustainable manufacturing systems. Int. J. Energy Res. 38 (6), 728–736.

Benavides, A.J., Ritt, M., 2018. Fast heuristics for minimizing the makespan in non-permutation flow shops. Comput. Oper. Res. 100 (December issue), 230–243.

Biel, K., Clock, C.H., 2016. Systematic literature review of decision support models for energy-efficient production planning. Comput. Ind. Eng. 101, 243–259.

Biel, K., Zhao, F., Sutherland, J.W., Glock, C.H., 2018. Flow shop scheduling with grid-integrated onsite wind power using stochastic MILP. Int. J. Prod. Res. 56 (5), 2076–2098.

Bilir, L., İmir, M., Devrim, Y., Albostan, A., 2015. Seasonal and yearly wind speed distribution and wind power density analysis based on Weibull distribution function. Int. J. Hydrogen Energy 40 (44), 15301–15310.

Chen, G., Zhang, L., Arinez, J., Biller, S., 2013. Energy-efficient production systems through schedule-based operations. IEEE Trans. Autom. Sci. Eng. 10 (1), 27–37.

Dong, X., Chen, P., Huang, H., Nowak, M., 2013. A multi-restart iterated local search algorithm for the permutation flow shop problem minimizing total flow time. Comput. Oper. Res. 40 (2), 627–632.

EIA, 2017. How much of U.S. carbon dioxide emissions are associated with electricity generation? US Energy. Inf. Adm. (EIA). Rep. available at: http://www.eia.gov/tools/faqs/faq.cfm?id=77&t=11 accessed September 29, 2018.

Fu, R., Feldman, D., Margolis, R., Woodhouse, M., Ardani, K., 2018a. The U.S. solar photovoltaic system cost benchmark: q1 2017. Natl. Renew. Energy. Lab. Rep. Available at: https://www.nrel.gov/docs/fy17osti/68925.pdf accessed September 21, 2019.

Fu, R., Remo, T., Margolis, R., 2018b. The 2018 U.S. utility-scale photovoltaics-plus-energy storage system costs benchmark. Natl. Renew. Energy. Lab. Rep. Available at: https://www.nrel.gov/docs/fy19osti/71714.pdf accessed on September 21, 2019.

Ghadimi, P., Kara, S., Kornfeld, B., 2013. Advanced on-site energy generation towards sustainable manufacturing. In: Re-engineering Manufacturing for Sustainability. Springer, Singapore, pp. 153–158.

Golpîra, H., Khan, S.A.R., Zhang, Y., 2018. Robust smart energy efficient production planning for a general job-shop manufacturing system under combined demand and supply uncertainty in the presence of grid-connected microgrid. J. Clean. Prod. 202, 649–665.

Hu, S., Chuah, Y., 2003. Power consumption of semiconductor fabs in Taiwan. Energy 28 (8), 895–907.

ITRS, 2011. Environmental, safety and health chapter. Report of international technology roadmap of semiconductors. Available. http://www.itrs2.net. accessed March 10, 2019.

Jin, T., Shi, K., Park, T., 2018. The quest for carbon-neutral industrial operations: renewable power purchase versus distributed generation. Int. J. Prod. Res. 58 (17), 5723–5735.

Lave, M., Kleissl, J., 2011. Optimum fixed orientations and benefits of tracking for capturing solar radiation. Renew. Energy 36 (3), 1145–1152.

Li, L., Sun, Z., 2013. Dynamic energy control for energy efficiency improvement of sustainable manufacturing systems using Markov decision process. IEEE Trans. Syst. Man Cybern. B Cybern. Syst. 43 (5), 1195–1205.

Liu, Y., Dong, H., Lohse, N., Petrovic, S., Gindy, N., 2014. An investigation into minimising total energy consumption and total weighted tardiness in job shops. J. Clean. Prod. 65, 87–96.

Liu, G.S., Zhang, B.X., Yang, H.D., Chen, X., Huang, G.Q., 2013. A branch-and-bound algorithm for minimizing the energy consumption in the PFS problem, 2013 Math. Probl. Eng. 1–6. https://doi.org/10.1155/2013/546810. available at:, accessed September 10, 2019.

Liu, Y., Farnsworth, M., Tiwari, A., 2018. Energy-efficient scheduling of flexible flow shop of composite recycling. Int. J. Adv. Manuf. Technol. 97 (1–4), 117–127.

Marichelvam, M.K., Prabaharan, T., Yang, X.S., 2014. Improved cuckoo search algorithm for hybrid flow shop scheduling problems to minimize makespan. Appl. Soft Comput. 19 (6), 93–101.

May, G., Stahl, B., Taisch, M., Prabhu, V., 2015. Multi-objective genetic algorithm for energy-efficient job shop scheduling. Int. J. Prod. Res. 53 (23), 7071–7089.

Mitra, S., Grossmann, I.E., Pinto, J.M., Arora, N., 2012. Optimal production planning under time-sensitive electricity prices for continuous power-intensive processes. Comput. Chem. Eng. 38 (5), 171–184.

Moon, J.-Y., Park, J., 2014. Smart production scheduling with time-dependent and machine-dependent electricity cost by considering distributed energy resources and energy storage. Int. J. Prod. Res. 52 (13), 3922–3939.

Mouzon, G., Yildirim, M.B., Twomey, J., 2007. Operational methods for minimization

of energy consumption of manufacturing equipment. Int. J. Prod. Res. 45 (18–19), 4247–4271.
Novoa, C., Jin, T., 2011. Reliability centered planning for distributed generation considering wind power volatilities. Electr. Power Syst. Res. 81 (8), 1654–1661.
Pham, A., Jin, T., Novoa, C., Qin, J., 2019. A multi-site production and microgrid planning model for net-zero energy operations. Int. J. Prod. Econ. 218, 260–274.
Ruangpattana, S., Klabjan, D., Arinez, J., Biller, S., 2011. Optimization of on-site renewable energy generation for industrial sites. In: Proceedings of IEEE PES Power Systems Conference and Exposition. PSCE), pp. 1–8.
Ruiz, R., Vázquez-Rodríguez, J.A., 2010. The hybrid flow shop scheduling problem. Eur. J. Oper. Res. 205 (1), 1–18.
Shrouf, F., Ordieres-Meré, J., García-Sánchez, A., Ortega-Mier, M., 2014. Optimizing the production scheduling of a single machine to minimize total energy consumption costs. J. Clean. Prod. 67, 197–207.
Stehly, T., Beiter, P., Heimiller, D., Scott, G., 2018. The 2017 cost of wind energy review. Natl. Renew. Energy. Lab. Rep. Available at: https://www.nrel.gov/docs/fy18osti/72167.pdf accessed September 21, 2019.
Taboada, H., Xiong, Z., Jin, T., Jimenez, J., 2012. Exploring a solar photovoltaic-based energy solution for a green manufacturing environment. Proc. IEEE. Conf. Autom. Sci. Eng. (CASE). 40–45.
Thiringer, T., Linders, J., 1993. Control by variable rotor speed of a fixed pitch wind turbine operating in a wide speed range. IEEE Trans. Energy Convers. 8 (3), 520–526.
Villarreal, S., Jimenez, J.A., Jin, T., Cabrera-Rios, M., 2013. Designing a sustainable and distributed generation system for semiconductor wafer fabs. IEEE Trans. Autom. Sci. Eng. 10 (1), 16–26.
Wan, G., Qi, X., 2010. Scheduling with variable time slot costs. Nav. Res. Logist. 57 (2), 159–171.
Wang, Y., Li, L., 2013. Time-of-use based electricity demand response for sustainable manufacturing systems. Energy 63 (December issue), 233–244.
WU, 2018. Weather Underground portal. Available at: http://www.wunderground.com/. accessed August 2, 2018.
Yenisey, M.M., Yagmahan, B., 2014. Multi-objective permutation flow shop scheduling problem: literature review, classification and current trends. Omega 45 (6), 119–135.
Zhang, H., Cai, J., Fang, K., Zhao, F., Sutherland, J.W., 2017a. Operational optimization of a grid-connected factory with onsite photovoltaic and battery storage systems. Appl. Energy 205 (November issue), 1538–1547.
Zhang, R., Chiong, R., 2016. Solving the energy-efficient job shop scheduling problem: a multi-objective genetic algorithm with enhanced local search for minimizing the total weighted tardiness and total energy consumption. J. Clean. Prod. 112 (4), 3361–3375.
Zhang, H., Zhao, F., Fang, K., Sutherland, J.W., 2014. Energy-conscious flow shop scheduling under time-of-use electricity tariffs. CIRP Ann. - Manuf. Technol. 63 (1), 37–40.
Zhang, Y., Islam, M.M., Sun, Z., Yang, S., Dagli, C., Xiong, H., 2018. Optimal sizing and planning of onsite generation system for manufacturing. Int. J. Prod. Econ. 206, 261–267.
Zhang, H., Zhao, F., Sutherland, J.W., 2017b. Scheduling of a single flow shop for minimal energy cost under real-time electricity pricing. J. Manuf. Sci. Eng. 139 (1), 5. https://doi.org/10.1115/1.4034275. Available at: